Available online at www.sciencedirect.com
ScienceDirect
Deep-Sea Research II 55 (2008) 1179–1194
DEEP-SEA RESEARCH PART II
www.elsevier.com/locate/dsr2

Eddy activity in the lee of the Hawaiian Islands

Paulo H.R. Calil[a,*], Kelvin J. Richards[a,b], Yanli Jia[b], Robert R. Bidigare[c]

[a]Department of Oceanography, University of Hawaii at Manoa, USA
[b]International Pacific Research Center, University of Hawaii at Manoa, USA
[c]Hawaii Institute of Marine Biology, University of Hawaii at Manoa, USA

Accepted 20 January 2008
Available online 19 May 2008

Abstract

Persistent northeasterly trade winds have a substantial impact on the oceanic circulation around the Hawaiian Islands. A regional ocean model is applied to understand the effect of different temporal and spatial resolutions of surface momentum forcing on the formation of strong mesoscale vortices and on the simulation of realistic levels of eddy kinetic energy. The higher spatial and temporal resolutions of wind forcing is shown to substantially affect the vorticity and deformation field in the immediate lee of the Hawaiian Islands and produce patterns of eddy kinetic energy similar to observations. This suggests that the surface eddy field in the region is mostly dominated by the local surface momentum forcing. Mesoscale cyclones and anticyclones formed in the lee of the Island of Hawaii are shown to have different propagation patterns. Mesoscale cyclones are more confined to the lee and are hence subject to interactions with the strong wind forcing and deformation field as well as smaller vortices formed in the wake of the other islands. Mesoscale anticyclones show not only a tendency to propagate further westward, but also to persist as coherent features as they propagate, even at relatively lower values of relative vorticity. The large strain rates that affect the propagation of the cyclones cause them to break down into filaments of positive vorticity. Rossby numbers of O(1) within vortices and filaments indicate that nonlinear interactions between the wind stress and the vertical component of the relative vorticity field is potentially important in producing large vertical velocities. Modeled cyclonic eddies show a good resemblance to observations both in terms of vertical structure and propagation patterns.

Keywords: Mesoscale eddies; Wind forcing; Mesoscale circulation; Numerical modeling

1. Introduction

The Hawaiian archipelago has a strong influence on both oceanic and atmospheric circulations. Persistent northeasterly trade winds of $5-10\,ms^{-1}$ flow throughout most of the year, with increased strength during the summer (Smith and Grubisic, 1993). The largest obstructions to the atmospheric flow are the Islands of Maui and Hawaii, whose peaks, Haleakala (3055 m) on Maui, and Mauna Kea (4201 m) and Mauna Loa (4169 m) on Hawaii, penetrate the trade-wind inversion layer extending from 1700 to 5000 m (Smith and Grubisic, 1993). Hence, winds flow around, rather than over, the obstacles, which creates a wake region of weak leeward winds. The funneling of the wind between the Islands of Maui and Hawaii is one of the key forcing mechanisms of cyclonic eddies observed in the region (Lumpkin, 1998).

Both cyclonic and anticyclonic mesoscale vortices are formed in the lee of the islands. After their formation, the anticyclones propagate west-southwestward and their signal can be observed at the Wake Islands, more than 4000 km west of Hawaii (Mitchum, 1995) as 90-day oscillations in sea-surface height anomaly (SSHA). The cyclones tend to propagate northwestward along the island chain, hence interacting with the secondary wakes and smaller scale eddies therein.

The mechanisms of formation and propagation of the lee eddies are still a matter of debate. The northeasterly trade winds impinge on the islands all year long, with stronger intensity and high spatial and temporal variabilities during increased trade winds. However, there is no conclusive study to date that demonstrates a higher frequency of eddy shedding during summer months, which would suggest a

*Corresponding author.
E-mail address: calil@hawaii.edu (P.H.R. Calil).

0967-0645/$ - see front matter © 2008 Elsevier Ltd. All rights reserved.
doi:10.1016/j.dsr2.2008.01.008

direct cause–effect relationship between wind forcing and eddy generation.

Given the clear importance of the local wind forcing on eddy generation, this study will focus on the extent to which the spatial and temporal resolutions of such a forcing affects the mesoscale variability observed in the lee of the islands. The fact that the middle of the subtropical gyre is typically a region of low productivity makes the study of any potential process that can enhance primary production in this region relevant. Mesoscale cyclonic eddies are important agents in bringing nutrient-rich waters at depth to the euphotic zone and hence, increasing biological activity (McGillicuddy and Robinson, 1997; Seki et al., 2001). The study of eddy formation and propagation in the Hawaiian region is crucial if we want to assess their relative importance to the ecosystem.

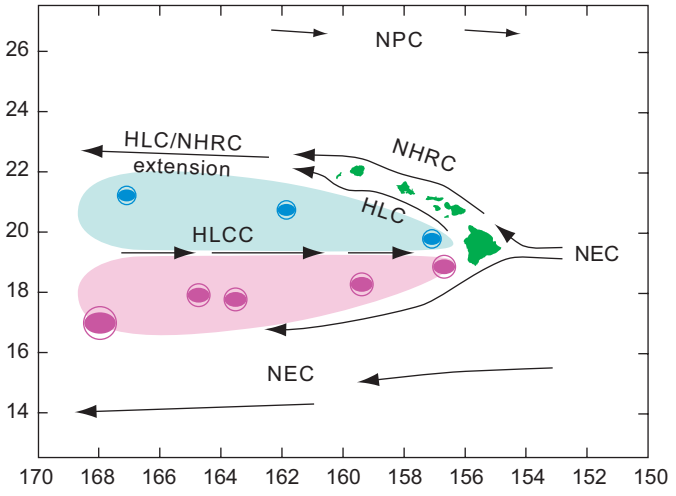

Fig. 1. Schematic diagram showing the main surface currents (see text for description) around the Hawaiian Islands as well as the predominant paths of cyclones (blue) and anticyclones (magenta). After Lumpkin (1998).

2. Background

The prevailing northeasterly trade winds and the spatial extent of the island chain create characteristic and relatively steady forcing of the ocean. A schematic diagram of the surface regional circulation is shown in Fig. 1. The vorticity input of the wind-stress curl associated with the Hawaiian Island wake is the main forcing mechanism of the Hawaiian Lee Counter Current (HLCC, Qiu et al., 1997; Xie et al., 2001). Centered around 19°N, the HLCC is an eastward-flowing current that advects warm water toward the lee of the Island of Hawaii. The interaction of the converging winds and warm sea-surface temperature (SST) along the zonal extent of the HLCC results in an extremely large wake region (Xie et al., 2001). On average, the circulation in the lee is composed of two quasi-steady rotating regions, cyclonic to the north and anticyclonic to the south, separated by the impinging HLCC.

Lumpkin (1998) reports the existence of the Hawaiian Lee Current (HLC), flowing west-northwestward along the southwest side of the islands with speeds as high as $0.2\,\mathrm{ms}^{-1}$, 150 km offshore. Along the northeast side of the islands and flowing northwestward is the time-varying North Hawaiian Ridge Current (NHRC), which behaves as a western boundary current in the context of the island rule (Godfrey, 1989). An 8-year mean of $0.15\,\mathrm{ms}^{-1}$ was obtained by Firing et al. (1999) when averaging data from 58 cruises in the region. The North Equatorial Current (NEC), which is the southern limb of the North Pacific subtropical gyre, flows westward south of the islands with speeds exceeding $0.25\,\mathrm{ms}^{-1}$.

The combination of the atmospheric and oceanic flows described above gives rise to an intense eddy field in the lee

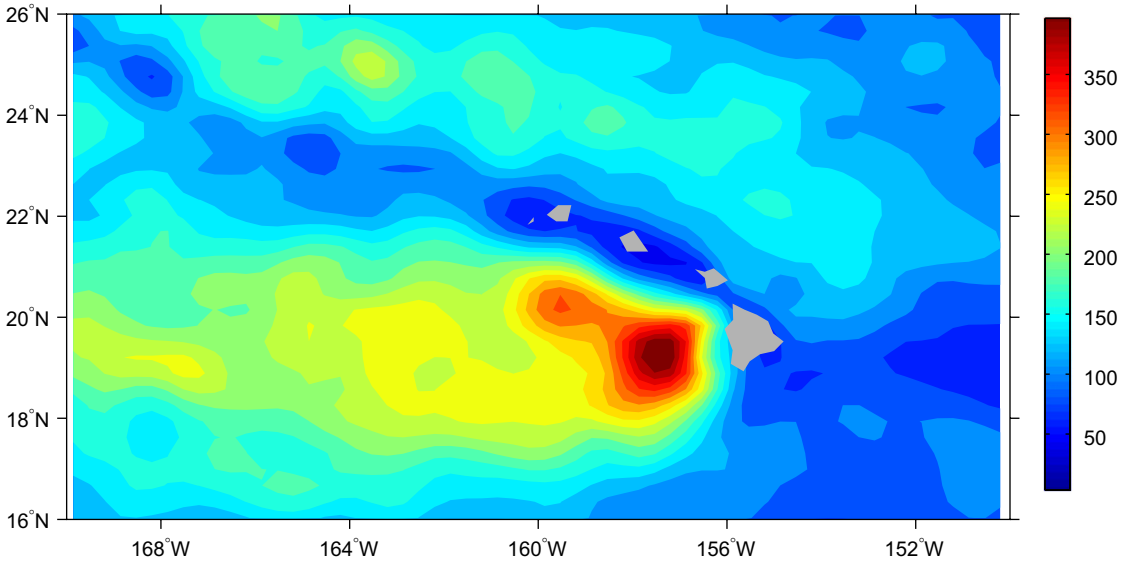

Fig. 2. Mean eddy kinetic energy $(\mathrm{cm/s})^2$, from 1992–2005. Calculated from TOPEX/ERS merged SSHA data.

of the islands. Mesoscale eddies are formed as a result of wind forcing and intrinsic instabilities of the oceanic flow. Fig. 2 shows a map of EKE calculated from SSHA data from the TOPEX/ERS dataset, a combined data product from TOPEX Poseidon, ERS and Jason1 satellites (resolution: 0.33° in longitude and 0.18° in latitude), between 1992 and 2005.

The largest signal in EKE is to the west of the Island of Hawaii, with a maximum at around 19°N, 157°W. The strong variability in the region is a result of a combination of wind forcing and instability of the NEC, which promotes the formation of mesoscale eddies in the immediate lee of Hawaii (Lumpkin, 1998; Flament et al., 2001). Cyclones *Opal* and *Noah*, sampled during the E-Flux project, were observed very close to the region of maximum EKE (Dickey et al., 2007; Kuwahara et al., 2007; Nencioli et al., 2007).

A secondary peak in EKE is seen at around 20°N, 160°W, which can be indicative of eddy activity in the secondary wakes of the Islands of Maui, Oahu and Kauai. High values of EKE also are observed in the region of the HLCC, further to the west. Seasonal variations of the deeper westward flow and the surface eastward flow can make the region baroclinically unstable. Strong vertical shear in the horizontal velocity and weak stratification in the region are thought to be the main mechanisms of instability (Kobashi and Kawamura, 2002). The region northeast of the Hawaiian Islands has a relatively small but robust EKE signal, compared to the values in the lee. Chen and Qiu (2006) argue that such a signal is a result of trapped annual Rossby waves, parallel to the island chain, and a basin-scale, non-propagating signal.

3. The model

The ocean model used in this study is the regional ocean modeling system (ROMS, Shchepetkin and McWilliams, 2005). ROMS is a free-surface, hydrostatic primitive-equation model, with a vertical terrain-following coordinate and horizontal curvilinear coordinates. It includes a new method for computing the pressure gradient in models with non-aligned vertical coordinates (Shchepetkin and McWilliams, 2003). To avoid errors associated with the steep topography of the Hawaiian Islands, ETOPO2 bathymetry (2 min gridded global relief data) is smoothed in order to maintain the slope parameter $r = \nabla h/h$, the ratio between the model resolution and the topographic variation (Beckmann and Haidvogel, 1993), less than 0.3.

The model domain ranges from 150°W to 170°W and from 16°N to 26°N. After sensitivity studies with lower resolution (not shown), we determined that a horizontal resolution of 1/12 degree (approximately 8.5 km) is an optimal balance between computational expense and the resolution of the mesoscale eddy field necessary to maintain sufficient model sensitivity to surface momentum forcing. Given that the Rossby deformation radius at the latitude of the Hawaiian Islands is between 50 and 60 km, we expect the model to resolve the mesoscale, but not the sub-mesoscale. There are 20 layers in the vertical. The stretching parameters of the s-coordinate vertical grid were adjusted in order to have a higher resolution in the upper ocean ($\theta_s = 7$, $\theta_b = 0$).

The model is forced with monthly surface heat and freshwater fluxes from the comprehensive ocean atmosphere data set (COADS). Thermal feedback of model surface temperature to surface heat flux is done through a correction term with respect to COADS SST (Marchesiello et al., 2003). The same procedure is applied to surface salinity because of the paucity of evaporation and precipitation data.

There are four open boundaries. Monthly climatological values of temperature and salinity from the World Ocean Atlas (WOA2001; Conkright et al., 2002) and the appropriate winds for each experiment were used to estimate the baroclinic component of the geostrophic and Ekman velocities, respectively. To determine the total velocity at the boundaries, a level of no motion at 1000 m depth was used. An oblique radiation condition was used to obtain the direction of the flux at the boundaries. In case of outflow, an active, implicit upstream-biased radiation condition was used to connect the model solution to the open boundaries (Shchepetkin and McWilliams, 1998; Penven et al., 2006). In case of inflow, the solution of the boundary was nudged toward climatological values (Marchesiello et al., 2001). For inflow, climatological values are quickly restored with a nudging timescale of 3 days. For outflow, the radiation condition and weak nudging (i.e. 360 days) were used to extrapolate interior values at boundary points. There is no explicit lateral viscosity within the model domain, except in the sponge layers near the open boundaries where it increases smoothly on a few grid points (Penven et al., 2005). Climatological values of the model variables were used for initialization and the model was run for 8 years.

4. Forcing fields

To examine the impact of the wind forcing resolution in the ocean model, we used monthly averages of three different wind products: (1) the 0.5° resolution climatological COADS winds; (2) a 0.25° resolution gridded QuikSCAT product produced by remote sensing systems and sponsored by the NASA ocean vector winds science team (data are available at www.remss.com); and (3) a blending of the 0.25° resolution QuikSCAT gridded product and the output of a mesoscale atmospheric model (MM5, whose domain is the state of Hawaii at 9-km resolution, Yang et al., 2005) using all available data for 2004–2006. As for the temporal resolution, a 3-day running mean of QuikSCAT, at daily intervals for 2005, was used repeatedly over the 8 years of model run. Wind stress was calculated from the velocity components using the bulk formula of Large and Pond (1981). We will refer to the monthly COADS run as COADS, the monthly QuikSCAT

run as QSMONTHLY, the QuikSCAT 2005 daily run as QSDAILY, and the blended run as BLENDED (see Table 1). Annual averages of wind stress curl for COADS, QSMONTHLY, and BLENDED on the model grid are shown in Fig. 3.

There are several processes that may negatively influence the QuickSCAT data used to force our model. For example, land contamination of QuikSCAT data occurs within 25–37 km (the minor and major axes of the ellipsoidal footprint) of the coast. In addition, noise is introduced in the gridded wind data through the complex spatial and temporal sampling of the scatterometer (Chao et al., 2003). Wind speed and direction are obtained from the normalized backscattered power through a geophysical model function that is related to the number of "looks" (i.e. adjacent points in which observations are available) in the footprint (Tang et al., 2004). Since there are no looks relatively close to the coast, the speed and the direction of the coastal data are based on measurements slightly offshore where the topography is not yet felt and the predominant wind direction is that of the northeasterly trade winds. It is an open question whether values close to the coast are significant to ocean dynamics.

To investigate this question further, we developed a blended product with monthly means of QuikSCAT and outputs of the atmospheric model, MM5 (Yang et al., 2005). The MM5 domain spans from 160.5°W to 153.5°W and from 18°N to 23°N, which is smaller than the ROMS domain. In order to utilize the much finer MM5 wind stress resolution close to the Hawaiian Islands without reducing the size of the domain, the two products were merged as follows.

Spatial averages of wind stress components for both MM5 and QuikSCAT over the MM5 domain are computed and subtracted from the original wind stress fields to obtain the wind stress anomalies. This is done to each of the monthly fields. For each field, a new anomaly is formed that consists of the QuikSCAT anomaly outward of the MM5 domain, a weighted combination of the QuikSCAT and MM5 anomalies from the MM5 boundaries inward over 10 model grid intervals (a transition zone of approximately 0.83°), and the MM5 anomaly inward of the transition zone. Finally, the spatial averages of QuikSCAT wind stress components are added to the newly formed anomaly fields to obtain the blended product used to force the ocean model. The result was a product with higher spatial resolution around the islands, with QuikSCAT data for the remainder of the domain.

Table 1
Summary of the surface momentum forcing fields

Forcing product	Horizontal resolution	Temporal resolution
COADS	0.5°	Monthly
QSMONTHLY	0.25°	Monthly
QSDAILY	0.25°	Daily (2005)
BLENDED	9 km/0.25°	Monthly

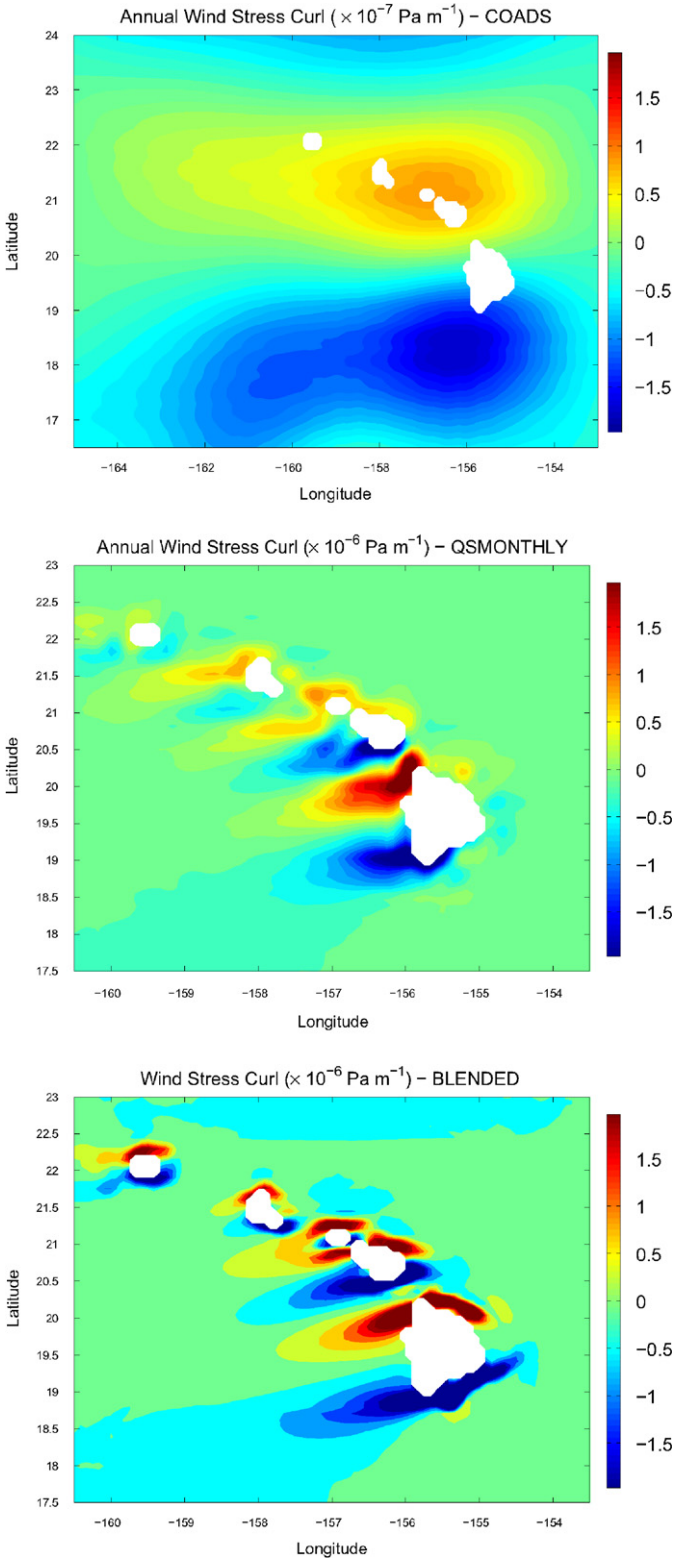

Fig. 3. Annual average of wind-stress curl for COADS (upper panel), QSMONTHLY (middle panel), and BLENDED (lower panel). Note that the values of the COADS plot are one order of magnitude smaller than the others. A different region was used in the upper panel in order to show the complete dipole structure.

Because of the coarser resolution and smoothing of the observations, the curl associated with COADS represents only the larger scale wind forcing around the islands, a dipole of large horizontal extent, with weak positive and negative curls on the northern and southern side of the domain, respectively (Fig. 3, upper panel). From this plot, there is no indication of individual island wakes. Minimum and maximum values are one order of magnitude lower that the other products (note the different scales used in Fig. 3 for better visualization). A different size of the region was selected in this case to show the complete dipole structure, while for the other products attention is paid to the spatial details close to the islands.

The 0.25° resolution QuikSCAT products reveal the detailed aspects of the individual wakes and, most strikingly, the very high values of wind-stress curl in the wake of the Islands of Maui and Hawaii. The minimum/maximum values for the climatological mean are $-2.6/2.9 \times 10^{-6}\,\mathrm{Pam}^{-1}$ (shown in Fig. 3), while for 2005 these are $-3.25/3.5 \times 10^{-6}\,\mathrm{Pam}^{-1}$ (not shown). Using the classical, linear Ekman pumping velocity formula

$$w_E = \frac{\nabla \times \vec{\tau}}{\rho_0 f}, \quad (1)$$

where τ is the wind stress, ρ_0 is the background density, and f is the Coriolis parameter; average Ekman pumping velocities range from 4 to $6\,\mathrm{md}^{-1}$. On a synoptic scale, such values may be much larger (Chavanne et al., 2002). The stronger values in QuikSCAT, are on the lee side with some slight perturbations on the windward side of the islands.

The wind-stress curl associated with the blended product has generally higher values than the QuikSCAT measurements. The minimum/maximum values for the annual average are $-7.3/5.1 \times 10^{-6}\,\mathrm{Pam}^{-1}$, with corresponding Ekman pumping velocities of $-12.3/8.6\,\mathrm{md}^{-1}$, respectively. Note that there are large values, although on a smaller scale, associated with each individual island. Large values of wind-stress curl are also seen on the windward side of the islands, associated with the deceleration and deflection of winds as they encounter topographic features. These values are not captured by the QuikSCAT measurements and can be either an over-estimation of the wind field by the atmospheric model or an under-estimation of QuikSCAT both because of averaging and/or land contamination. The former scenario is unlikely since the atmospheric model topography is smoothed, and orographic effects would be, in this case, underestimated (Hafner and Xie, 2003).

5. Model results

5.1. Mean surface velocity fields

Annual mean surface-flow fields for all experiments are shown in Fig. 4. All agree satisfactorily with the previous

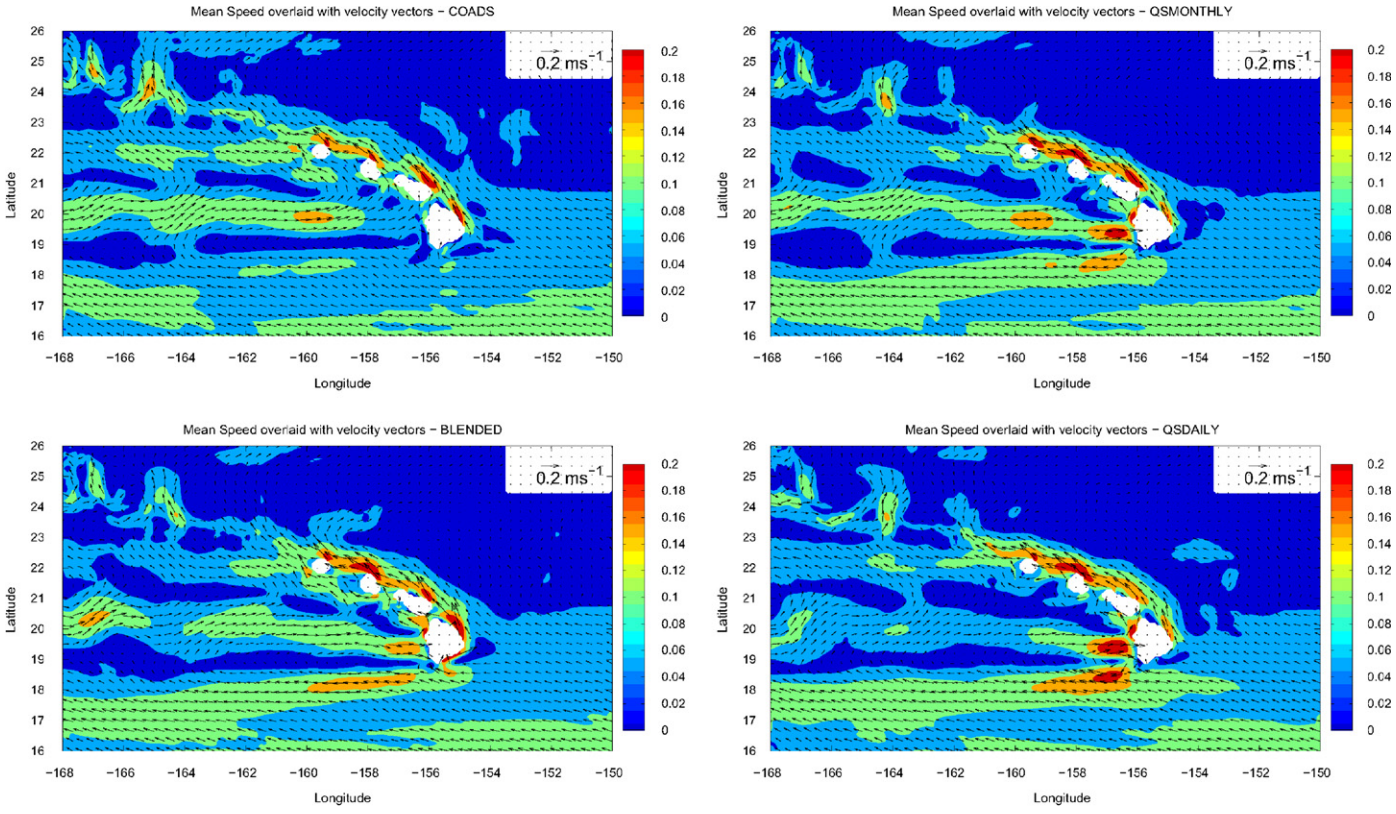

Fig. 4. Annual average (calculated from model years 4 to 8) of modeled surface horizontal velocity for COADS (upper left), QSMONTHLY (upper right), BLENDED (lower left), and QSDAILY (lower right).

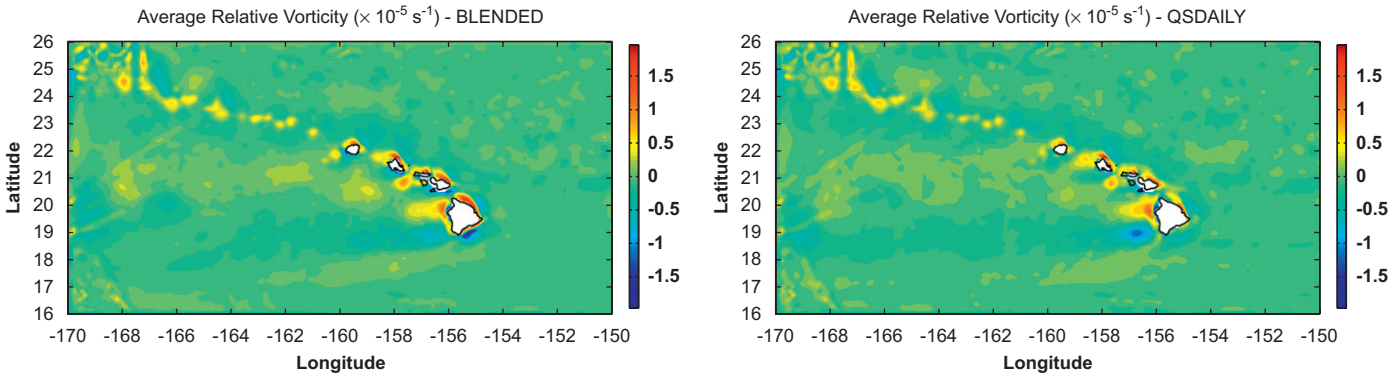

Fig. 5. Average surface relative vorticity calculated from the annual average of horizontal velocity for BLENDED (left) and QSDAILY (right). Note the enhancement of anticyclonic mean relative vorticity southeast of Hawaii in the BLENDED run.

estimates of the surface circulation from drifters (Qiu et al., 1997, Fig. 5), showing the NHRC northeast of the island chain, the HLCC flowing eastward toward the lee of the islands and the NEC flowing westward on the southern portion of the domain. The HLC is stronger using the BLENDED wind fields because of the higher resolution near the coast. Overall, the experiments qualitatively reproduce the average surface circulation depicted in Fig. 1.

Differences occur near the coast of Hawaii, with higher surface velocities in QSDAILY and QSMONTHLY. Relative vorticity calculated from the mean fields for QSDAILY and BLENDED show that there is a mean cyclonic field in the northern part of the wake of Hawaii, centered around 19°N and an anticyclonic mean field south of that region (Fig. 5). Those regions coincide with the regions of formation and intensification of cyclonic and anticyclonic lee eddies, respectively. Higher mean relative vorticity values for the BLENDED run near the coast are a consequence of the higher resolution of the MM5 runs than QuikSCAT measurements in these regions, particularly to the southeast (northeast) of Hawaii, where the mean anticyclonic (cyclonic) vorticity is enhanced as a response to the strong negative (positive) wind-stress curl (see Fig. 3, bottom). Average vorticity for QSMONTHLY (not shown) was similar to QSDAILY, while COADS was characterized by very low values.

Another important difference is the strength and location of the HLCC. COADS, in particular, has a quasi-zonal counter-current at 20°N, slightly displaced to the north relative to other runs, due to the large dipole (Fig. 3, top).

5.2. Eddy kinetic energy

The same procedure applied to calculate EKE from satellite data (Fig. 2) was employed in the model runs from the model free surface. Maps of model EKE, averaged from years 4 to 8, are shown in Fig. 6. EKE values from all experiments, except for COADS, show good agreement with the observations (Fig. 2). With COADS winds, values are much lower than observed and there is no clear maximum in the lee of the islands. EKE values are slightly higher in the region of the HLCC, showing that the larger scale dipole of wind-stress curl, although weaker than observed, is able to induce a counter-current. This is also corroborated with the surface velocity maximum shown in Fig. 4 (upper left). Notice that the latitude of the HLCC in COADS corresponds to the region with zero wind-stress curl at about 20°N (Fig. 3, top).

The 5-year average of the model run forced with daily 2005 QuikSCAT data overestimates the values calculated from the altimeter measurements, which might not fully capture the local eddy variability because of its low resolution (0.33° in longitude and 0.18° in latitude). Interestingly, a secondary maximum in EKE is centered at 19.5°N, 159.5°W. This confirms the importance of high temporal wind forcing resolution, as no EKE secondary maximum is observed in the other runs (forced with monthly means). Although QSDAILY is a product of the winds for a single year, there is an ageostrophic current associated with the time derivative of the wind, in the direction of the wind when it strengthens and opposite to the winds when it weakens (McCreary et al., 1989). The secondary EKE maximum might be a consequence of the variability associated with this ageostrophic component.

The QSMONTHLY and BLENDED runs have very similar EKE fields, with a maximum in the immediate lee of Hawaii. The BLENDED and QSDAILY runs show larger values in the northeastern region, but still much smaller than observed levels. These results suggest that the circulation in the lee of the islands is strongly affected by local forcing while in the region northeast of the island chain, remote forcing mechanisms, such as annual Rossby waves, as suggested by Chen and Qiu (2006), are probably important as well. Such remote mechanisms are absent in our simulations because the model is restored to climatological values at the boundaries. The differences outlined above highlight the importance of high spatial and temporal resolutions of the surface momentum forcing field in reproducing realistic levels of EKE.

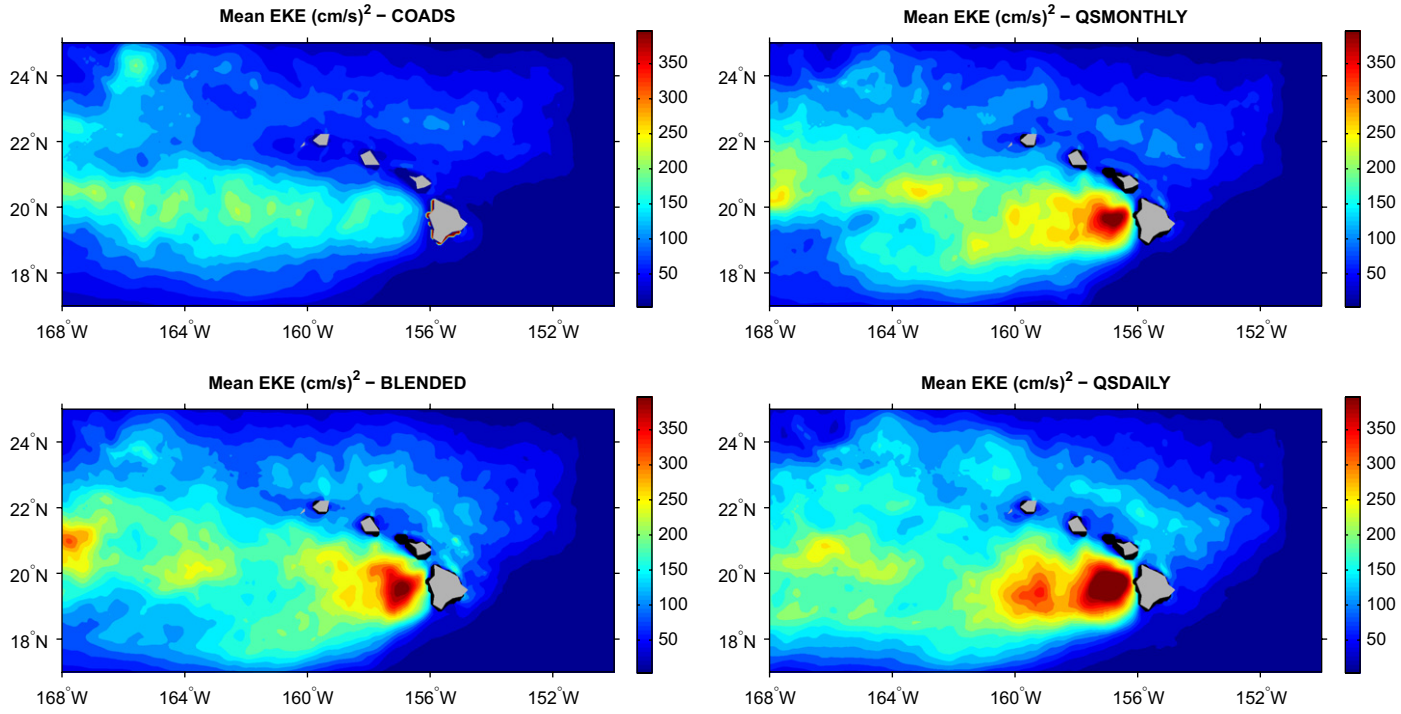

Fig. 6. Mean EKE (cm/s)^2 averaged from model years 4 to 8 for COADS (upper left), QSMONTHLY (upper right), BLENDED (lower left), and QSDAILY (lower right).

6. Mesoscale eddies

6.1. Comparison between modeled and observed eddies—vertical and horizontal structure

Although our model simulations were not designed to reproduce any specific observed eddy event, it is important to assess the capability of the model by comparing our results with observational data. We will base such comparisons with Cyclone *Opal* (Nencioli et al., 2007), sampled during E-Flux III cruise.

Cyclone *Opal* (Fig. 7), was sampled as part of the E-Flux project, an interdisciplinary collaboration designed to investigate the physics, biogeochemistry, and biology of cyclonic eddies that form in the lee of the Hawaiian Islands (Benitez-Nelson et al., 2007; Dickey et al., 2007). Cyclone *Opal* was intensively sampled during the E-Flux III cruise in March 2005 (see Nencioli et al., 2007 for physical details). Briefly, Cyclone *Opal*, was a well-developed 160-km-wide feature with significant surface expression, a maximum velocity of around 0.8 ms^{-1} and a vertical isothermal uplift of, approximately, 150 m at its core.

When it comes to the modeled eddies, the lower resolution wind product of the COADS run did not allow the model to produce significant isolated mesoscale cyclonic eddies. Some weak anticyclones were formed, an indication that instability processes might contribute to their formation, as suggested in the previous studies (Lumpkin, 1998; Flament et al., 2001). The low values of EKE in the COADS run (Fig. 6) further corroborates this conclusion. Therefore, the following discussion focuses on the QSMONTHLY, BLENDED, and QSDAILY model runs.

Strong cyclonic eddies were selected based on their maximum strength (i.e. vorticity, SST signal, and uplift of the isopycnals). SST maps as well as vertical sections of temperature and velocity taken at the center of each of these eddies are shown in Fig. 8. Note that strong cyclones occurred at different times of the year, thus the temperature differences in these comparisons are due to seasonal variability.

Maximum horizontal velocities and uplift of the isopycnals are around 0.6 ms^{-1} and 80–100 m in the QSDAILY and BLENDED model runs, respectively. Both eddies are symmetric and surface-intensified, with higher velocities confined to the upper 300 m. In the QSDAILY example, there seems to be a deeper influence of the cyclone as seen in the vertical extent of the zonal velocity. Note, however, that these are single events and might not be representative of the ensemble of eddies formed in each run. For the QSMONTHLY run, the eddies were generally weaker than the other two runs, which is explained by the fact that QSMONTHLY lacked both high spatial resolution in the region of strong wind-stress curl, similar to the BLENDED model, and the higher temporal resolution of the QSDAILY run.

6.2. Relative vorticity

As described previously, the mean circulation in the region west of Hawaii is composed of two quasi-steady

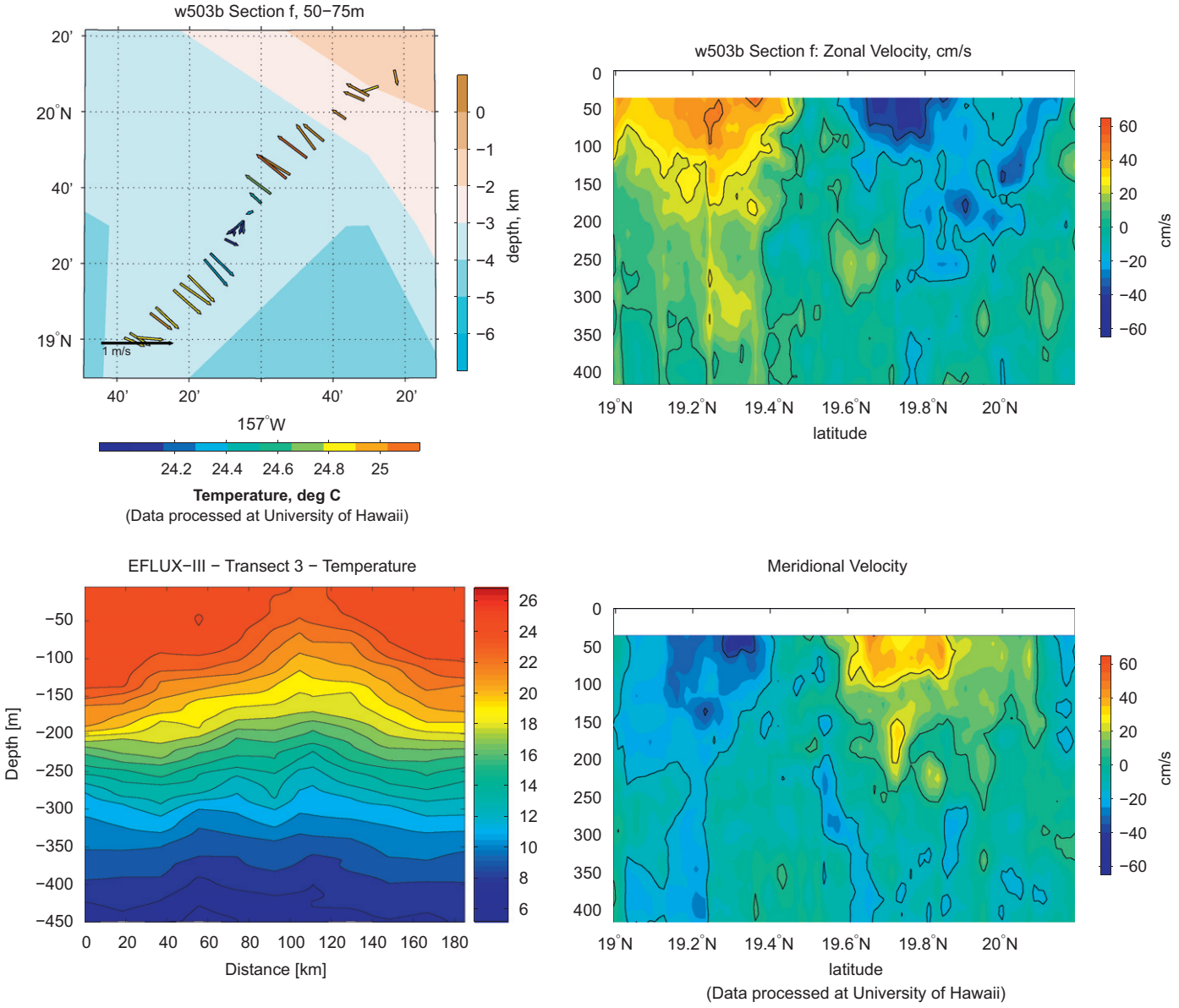

Fig. 7. Surface velocity vectors with colors representing temperature across Cyclone *Opal* at 50 m depth (upper left), as observed in the third cruise of the E-Flux project, from March 10 to 28, 2005. Temperature transect across Cyclone *Opal* (lower left). Maximum isotherm lifting is around 140 m. The right panel shows zonal and meridional velocity transects. The structure of the cyclone is mainly confined to the upper 250–300 m.

counter rotating gyres, cyclonic to the north and anticyclonic to the south. The northern (southern) part is associated with the region of positive (negative) wind-stress curl, hence Ekman suction (pumping), and cyclonic (anticyclonic) eddy generation.

Given the low EKE and absolute values of relative vorticity for the COADS run, it is not surprising that strong, locally generated mesoscale eddies were absent. Hence we focus on the resulting relative vorticity fields from the runs forced with QuikSCAT winds and the blended product.

Fig. 9 (left column) shows snapshots of the relative vorticity field for the same runs and the same dates as those shown in Fig. 8. A common feature is the persistence of the anticyclones after their formation, as seen by the strong negative areas to the west-southwest of the island chain. The anticyclones are surrounded by regions of cyclonic vorticity. The cyclones, although strong, seem to be confined to the immediate lee of the islands, as the positive regions break down into filaments of positive vorticity after strong cyclonic eddy events.

This behavior can be a result of the interaction with the secondary wakes of the smaller islands, which also shed less intense meso-, and possibly, submesoscale eddies of both signs. Also, by being more stationary, the cyclones would be subject to the strong, frequent wind pulses in the immediate lee, which could affect their coherency and strength.

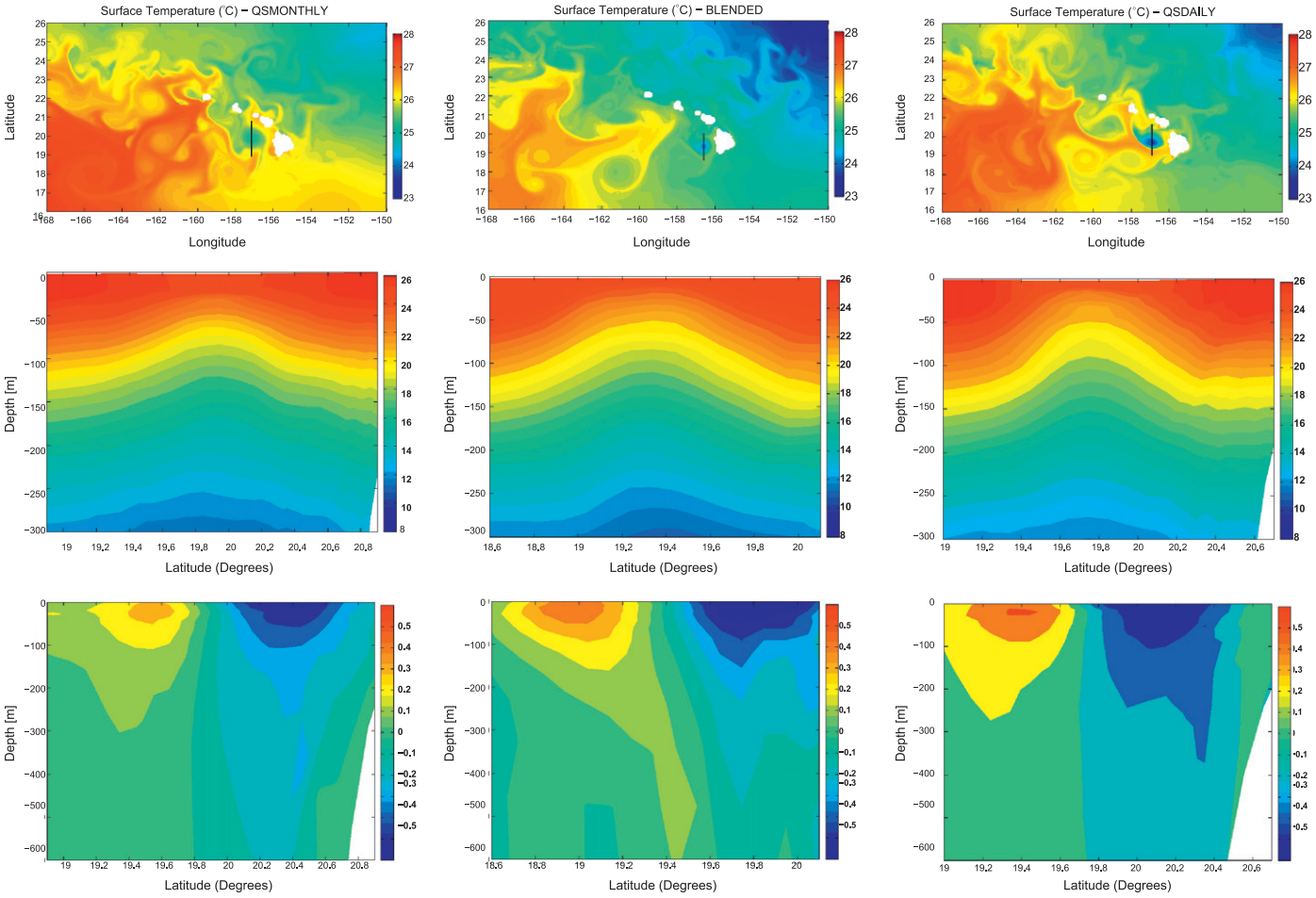

Fig. 8. *Upper panel*: Snapshots of SST for the model forced with QSMONTHLY (left), BLENDED (middle), and QSDAILY(right). The dates were chosen so that the cyclonic lee eddies were at their maximum strength before starting to decay. Vertical lines correspond to the meridional transects of temperature (in °C) (middle panel) and zonal velocity (in ms^{-1}) (lower panel) across the center of the eddies. See text for discussion. Note that strong eddies occurred at different times of the year for the different runs.

The only run in which the cyclones maintain their coherence further west of the islands is the one forced with QSMONTHLY winds. In this case, the vortices tend to split after a significant increase in radius. This difference in behavior between cyclones and anticyclones is further elucidated by the plots of the Okubo–Weiss parameter (Okubo, 1970; Weiss, 1991) shown in the right-hand-side panels of Fig. 9. The parameter is defined as the difference between the square of the deformation (or strain) and the square of the vertical component of the relative vorticity. Patches of intense, negative values of the Okubo–Weiss parameter are seen within the core of coherent vortices, meaning that these regions are vorticity dominated. On the boundaries of these features, intense, positive values are found, meaning that these regions are strain dominated.

Vorticity-dominated regions associated with anticyclones are more prominent further west of the islands. Note that the preferred region of formation of the cyclonic eddies is the region where the strain values are higher. The exception is the QSMONTHLY run, where the cyclones, although weaker, tended to be larger, more circular and maintained their coherence for longer time periods. They also had a tendency to propagate further northwestward than in the other runs. This suggests that high strain values, e.g., QSDAILY and BLENDED, had a higher impact on the cyclones formed in that region, preventing them from coherently propagating to the northwest, along the island chain. These results are further in agreement with Graves et al. (2006), who focused on interior vortices away from boundaries, that cyclones are weakened by a more robust strain field than anticyclones. These conclusions are also corroborated by the strength of the typical cyclones for each run (shown in Fig. 8). Since regions of strong vorticity and strain are entwined, in the run with weaker cyclones (i.e. QSMONTHLY) they are less affected by a strong strain field, hence able to maintain their coherence for longer periods.

In order to evaluate the strength and periodicity of modeled cyclones and anticyclones, two regions of the wake were selected. The region associated with positive vorticity ranged from 19.5°N to 20.5°N and from 156.5°W to 157.5°W and the region associated with negative

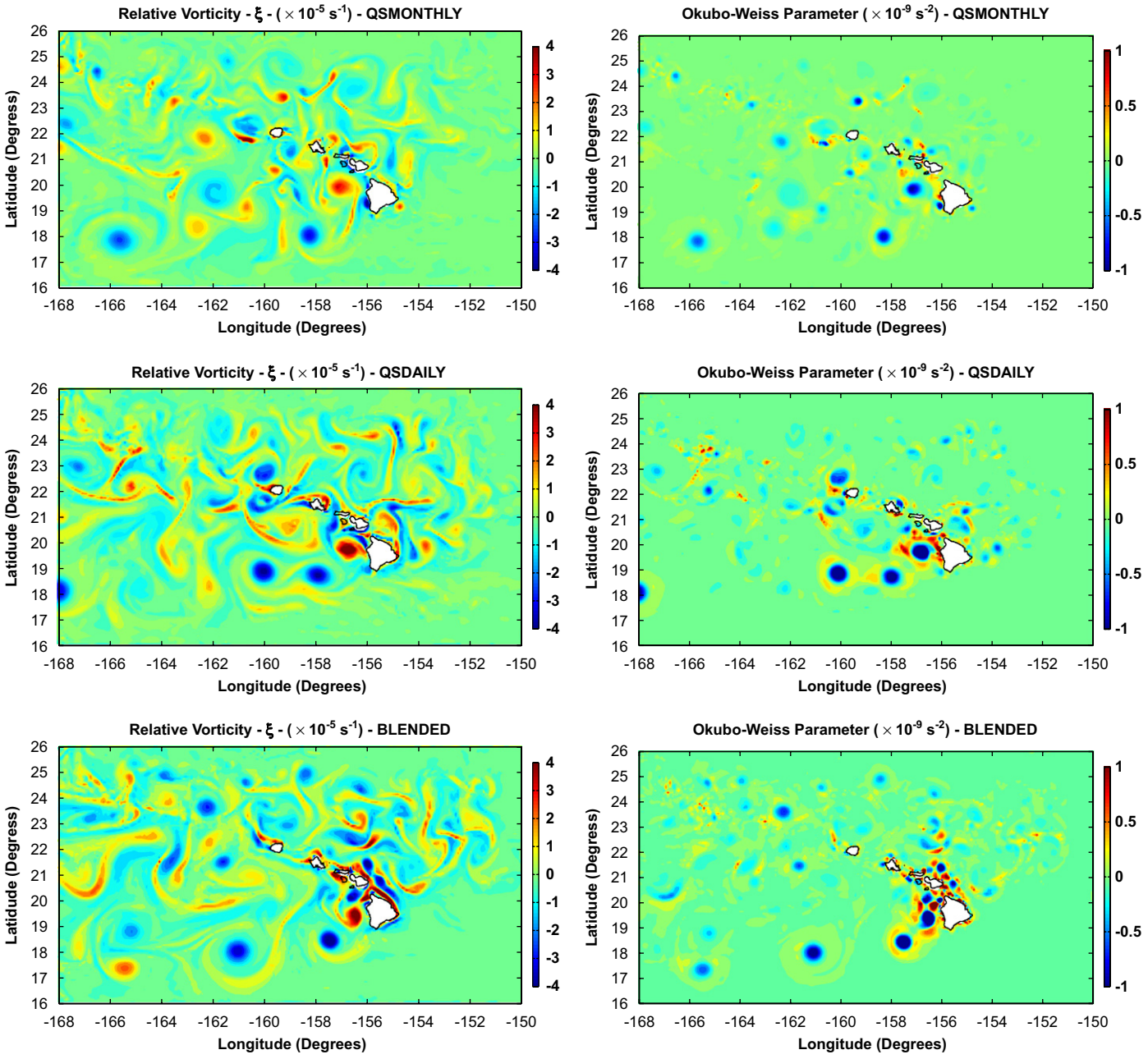

Fig. 9. Snapshots of relative vorticity (left column) and Okubo–Weiss parameter (right column). The selected dates were the same as for Fig. 8, when strong cyclones were formed in the lee of the islands, for QSMONTHLY (upper panel), QSDAILY (middle panel), and BLENDED (lower panel). Values for the COADS run are not shown because of the low values of vorticity (see Fig. 10).

vorticity extended from 18.5°N to 19.5°N with the same zonal extent. Relative vorticity was calculated from a 6-day average of the horizontal velocities for the model years 4–8, in order to capture only the more persistent features. In the northern (southern) region the negative (positive) values were removed and the maximum (minimum) values of relative vorticity selected. To avoid extreme values not associated with vorticity regions additional care was taken to remove values of strain-dominated regions (i.e. positive Okubo–Weiss parameter). Time-series of the maximum and minimum values for each run, normalized by the Coriolis parameter at 20°N (i.e. a local Rossby number), are shown in Fig. 10. The horizontal lines in the time-series plots correspond to the mean normalized vorticity value. A summary of mean values and standard deviations of maximum relative vorticity is given in Table 2.

Low mean and standard deviations of relative vorticity were obtained in the COADS run (Fig. 10, upper left). In terms of the mean values of relative vorticity, there is little difference between the anticyclonic and cyclonic sides of the wake in QSDAILY and QSMONTHLY, but the standard deviation is higher in the anticyclonic side in these

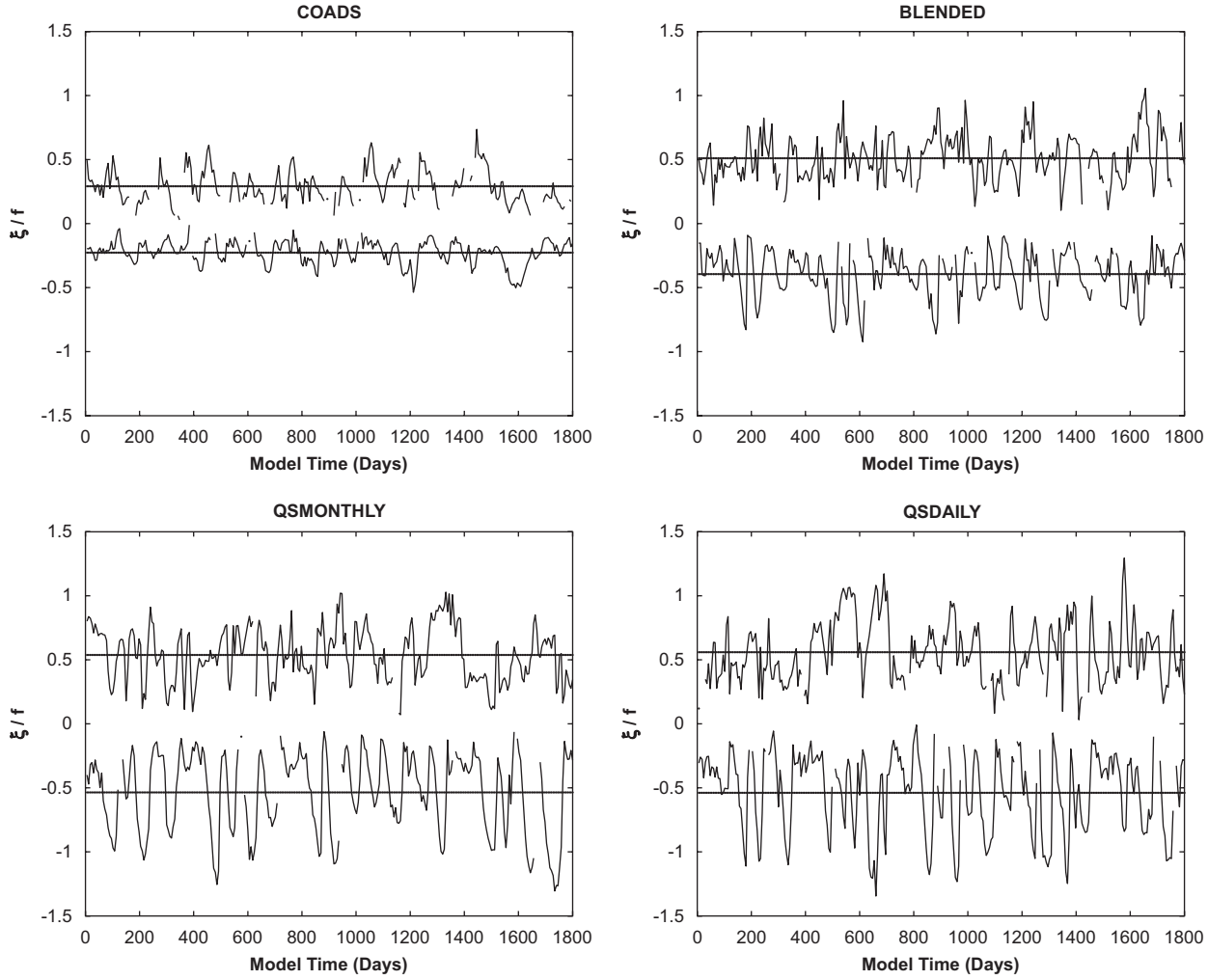

Fig. 10. Time-series of maximum/minimum of relative vorticity, in s^{-1}, in the region just west of the island of Hawaii (from 19.5°N to 20.5°N and from 156.5°W to 157.5°W, for the cyclonic region and from 18.5°N to 19.5.5°N, for the anticyclonic region, with the same zonal extent). Model time is in days, starting from model year 4. Relative vorticity values were normalized by the Coriolis frequency at 20°N.

runs, a consequence of the more frequent extremes in anticyclonic relative vorticity. In the BLENDED case, the mean value of cyclonic relative vorticity is larger than the anticyclonic. This effect is caused by the increased resolution near the coast which enhances anticyclonic vorticity southeast of Hawaii and diminishes, on average, the anticyclonic vorticity in the southern part of the wake (Fig. 5).

Time-series analyses indicate that cyclones tend to be more stationary, with persistently high relative vorticity for time periods of 60–100 days. In contrast, anticyclones seldom persist in the lee region. In other words, cyclones tend to be "trapped" to the lee of the islands, which is confirmed by observational evidence (Kuwahara et al., 2007; Nencioli et al., 2007) while anticyclones are not. Although the power spectra of the time-series (not shown) did not show any significant peaks, a rough estimate of eddy-shedding can be made simply by dividing the time range and the number of strong peaks. In QSDAILY, for example, 20 peaks (i.e. relative vorticity values above average) were observed in the 5-year period shown in Fig. 10. This yields a period of anticyclone formation of 91 days, remarkably similar to the 90-day oscillations referred to by Mitchum (1995) as the signal of the lee anticyclones at Wake Islands. In the case of the cyclones, such a calculation may be misleading because of their tendency to persist for longer times in the immediate lee.

Table 2
Mean and standard deviation of relative vorticity maxima associated with each region

Run	Cyclonic Vort. (s^{-1})		Anticyclonic Vort. (s^{-1})	
	Mean	Std. dev.	Mean	Std. dev.
COADS	1.45×10^{-5}	6.36×10^{-6}	-1.13×10^{-5}	4.56×10^{-6}
QSMONTHLY	2.67×10^{-5}	1.04×10^{-5}	-2.66×10^{-5}	1.54×10^{-5}
BLENDED	2.53×10^{-5}	8.73×10^{-6}	-1.96×10^{-5}	9.06×10^{-6}
QSDAILY	2.78×10^{-5}	1.17×10^{-5}	-2.67×10^{-5}	1.52×10^{-5}

In the BLENDED and QSDAILY cases, strong vortices of both signs have local Rossby numbers ($Ro = \xi/f$) equal or larger than unity, showing that ageostrophic and nonlinear processes can affect vortex formation and evolution. From the similar mean values of extrema of cyclonic and anticyclonic vorticity in the immediate lee no clear asymmetry can be seen, which implies that asymmetric properties arise from the differences in propagation and decay of cyclones and anticyclones.

6.3. Vortex evolution

In order to gain insight into the distinct behavior of cyclones and anticyclones, six strong vortices, formed at different times, were selected in the QSDAILY run, which has the best combination of temporal and spatial resolutions. The maxima in relative vorticity of each eddy was followed from the moment of detection until coherency was lost either by dispersion (i.e. increase in radius and loss of intensity) or breakdown into small filaments of relative vorticity (cyclones only).

The chosen vortices have diameters ranging from 80 to 120 km. The anticyclones tended to grow, intensify, and then decay as they propagated westward at speeds of $4.5-8.5\,\mathrm{km\,day^{-1}}$. The lower limit is similar to the long Rossby wave speed, frequently associated with the zonal drift of linear eddies. The higher values are possibly a consequence of advection by the westward flow of the NEC (Lumpkin, 1998). Maximum values of relative vorticity generally occur in the center of anticyclones and their shape is mainly circular. Cyclones, on the other hand, tend to "wobble"in the lee of the islands as they tended to be smaller and subject to stronger wind forcing and strain fields. Their shape was irregular and re-intensification often occurred.

Fig. 11 shows the evolution of the vorticity maxima, normalized by f at 20°N, within the individual eddies (left) and their paths (right). The initial intensification of anticyclones reaches a limit when the maximum values exceed $-f$. This may be an evidence of centrifugal instability (Dong et al., 2007), in accordance with the previous observational studies that suggested that the unstable anticyclone shear layer grows rapidly to a width set by the centrifugal stability condition (Flament et al., 2001). The paths of the anticyclones are characterized by a west-southwest propagation, with deviations such as the southward motion of AC2 or the northwest motion AC3 likely due to interactions with the NEC and the HLCC as well as other mesoscale eddies.

Cyclones behave quite differently. Maximum values in relative vorticity are characterized by sudden peaks, which appear related to changes in shape, diameter, wind driven intensification, and interactions with smaller eddies in the secondary wakes. Their propagation patterns vary. CYC1 forms in the lee of Hawaii and propagates west-southwest before moving to the northwest. CYC2 and CYC3, on the other hand, are essentially stationary for 4–6 months and never leave the immediate lee. As a result, they are subject to substantial forcing and strain fields which cause them to eventually break down into thin filaments of relative weak vorticity. This "stationary behavior"of the cyclones is substantiated by observational evidence (Kuwahara et al., 2007). The Rossby number of the eddies while in the immediate lee is often O(1), which implies that nonlinear, ageostrophic effects likely play a role in the way cyclonic eddies respond to wind forcing and the strain field as well.

6.4. Upstream effects

We have not considered the impact of eddies that propagate into the region from the east (Lukas and

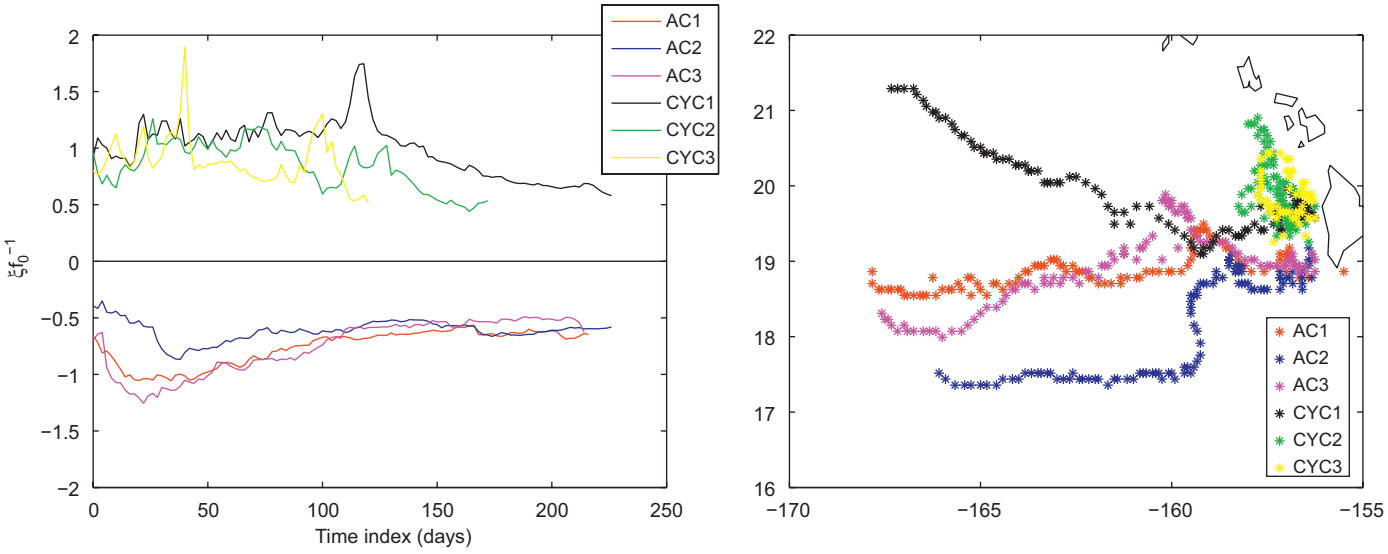

Fig. 11. Left: Evolution of extreme relative vorticity (normalized by the Coriolis parameter at 20°N) within three cyclones and three anticyclones formed at different times in the QSDAILY run. Right: Geographical paths of the selected eddies.

Santiago-Mandujano, 2001). To illustrate their potential effect, we examined a strong cyclone that formed in the ocean interior and impinged on the southern part of the island of Hawaii in March 2005 (based on TOPEX/ERS altimetry data, Fig. 12). During this period, a secondary minimum in SSHA, corresponding to Cyclone *Opal*, is also seen in the lee of the island. From this sequence of images, we can conclude that external variability (i.e. not generated in the lee) might also act to influence locally generated variability as well as affect the formation, propagation, decay, and possibly the biological impact of the lee eddies.

7. Discussion and conclusions

In this paper we have tested the sensitivity of a regional ocean model to different surface momentum forcing fields

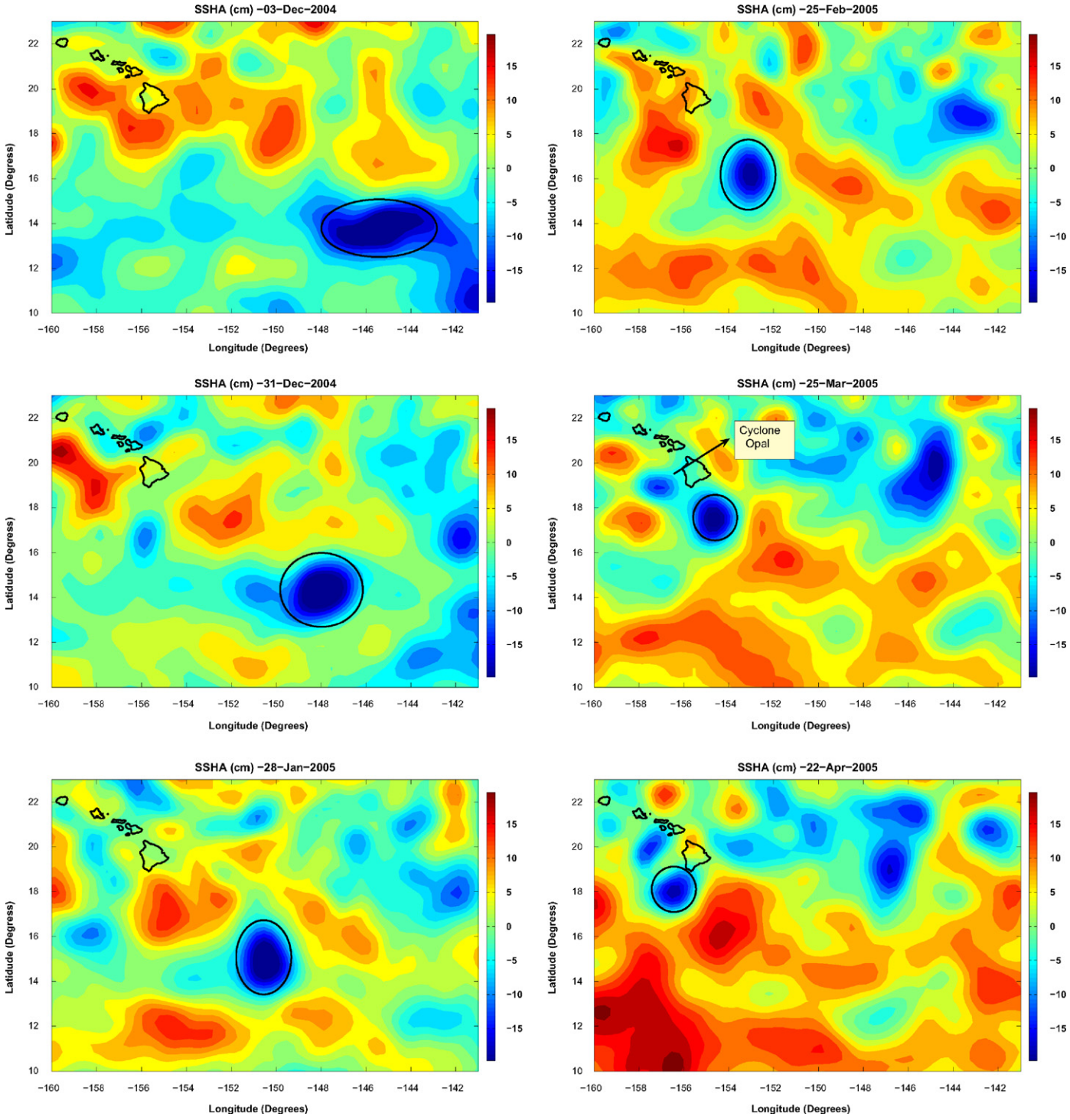

Fig. 12. Sequence of SSHA contour plots from TOPEX altimetry showing the propagation of a strong cyclone (annotated with an ellipse) toward the lee of the islands. The extraneous cyclone impinges on Hawaii and possibly interacts with Cyclonic lee eddy, Cyclone *Opal*.

around the Hawaiian Islands. Given the high variability of the wind in the region, its importance in forcing regional ocean circulation was demonstrated. The model results show that having high temporal and spatial resolution surface momentum forcing is vital to produce realistic levels of surface EKE and vorticity fields. QSMONTHLY and BLENDED showed very similar results, implying that on a monthly basis the added spatial resolution does not increase the local variability when compared to the coarser QuikSCAT data. Future studies with both higher temporal and spatial resolutions are needed in order to quantify the contribution of spatial resolution of wind forcing around the islands. QSDAILY showed realistic EKE values. More importantly, the secondary maximum in EKE resembles the observed pattern, showing that the increased temporal variability is significant for regional ocean circulation. From our results we conclude that higher EKE in the lee of the islands is locally generated (Fig. 6). The inability of the model to produce a broad region of high EKE values northeast of the islands support the conclusion of Chen and Qiu (2006) that this variability is generated by remote processes, such as annual Rossby waves.

7.1. Cyclone–anticyclone asymmetry

Our model results show a symmetric response in vorticity in the immediate wake (i.e. closer to the islands. See Fig. 10 and Table 2), with the notable exception of the BLENDED run, where anticyclonic vorticities are diminished in the lee and enhanced southeast of Hawaii (Fig. 5). The subsequent evolution, however, is asymmetric. Cyclones tend to linger in the lee of Hawaii and tend to succumb to exterior deformation and/or wind forcing field, developing smaller-scale filaments of positive vorticity. Anticyclones shed off the immediate wake and propagate west-southwestward while becoming more coherent (as seen by the more frequent peaks in anticyclonic vorticity in Fig. 10 as well as the vortex evolution pattern shown in Fig. 11).

There are a number of possible reasons for this asymmetry. As seen in Fig. 9, the region close to the channel between Maui and Hawaii is strain dominated. This is the preferential region of formation of cyclonic eddies. Graves et al. (2006), in the context of a shallow-water model with asymmetric and gradient-wind (a.k.a. cyclogeostrophic) balance, show that cyclones with length scales comparable to the deformation radius are more susceptible to decay under the influence of strong strain rates when the Rossby number is not small. As seen in Figs. 10 and 11, the local Rossby number of the modeled cyclones can be larger than unity. Along with the modeled high values of strain rates, this effect could be a key reason for the persistence of strong anticyclones.

McCreary et al. (1989) studied the response of the coastal ocean to strong offshore winds. They compared the response of a linear 1.5-layer model and a nonlinear 1.5-layer model to symmetric wind forcing. Their nonlinear model, which allows for entrainment, presents an asymmetric response favoring anticyclones. Entrainment of cool waters into the upper layer weakens cyclones while anticyclones are strengthened by advection terms.

Nonlinear Ekman effects also might play an important role in the asymmetric response of the ocean to wind forcing. For flows where the Rossby number is not small, the relative vorticity of a pre-existing, interior flow interacts with wind stress such that the Ekman transport is inversely proportional to the absolute vorticity ($A = \xi + f$, where ξ is the vertical component of the relative vorticity of a pre-existing flow, Stern, 1965; Niiler, 1969; Thomas and Rhines, 2002). In this scenario, Ekman transport would be diminished (enhanced) in regions of cyclonic (anticyclonic) interior vorticity.

7.2. Importance of the submesoscale

The present study is largely descriptive in terms of the sensitivity of a regional ocean model to wind forcing. The study does, however, demonstrate the influence of both spatial and temporal scales of the forcing in driving the eddy flow in the lee of the Hawaiian Islands. A detailed study of the dynamics will be the subject of a future paper. Preliminary work, however, suggests a potentially strong impact on wind forcing and submesoscale features.

Intense vertical motion, associated with submesoscale frontal dynamics, is thought to be responsible for a substantial amount of fluid exchange between the surface and nutrient-rich waters below the thermocline, with the wind having a crucial role in sustaining the submesoscale structure (Mahadevan and Tandon, 2006). Large vertical velocities are associated with high rates of strain, relative vorticity and loss of geostrophic balance (Mahadevan and Tandon, 2006). One of the mechanisms that is thought to enhance vertical motion in flows with a finite Rossby number is the aforementioned nonlinear Ekman pumping. Although our simulations do not resolve the submesoscale, the vorticity maps suggest a tendency for filamentation. The vigorous strain field, the horizontal shear associated with the wake, the high spatial and temporal variabilities of local winds as well as interactions among the vortices are all indications that smaller-scale (i.e. submesoscale) processes, in conjunction with the mesoscale, are important mechanisms of vertical fluid exchange in the lee of the Hawaiian Islands. Such features, together with their impact on the ecosystem, deserve future study.

Acknowledgments

We thank Dr. Yi-Leng Chen for the MM5 model data. Jules Hummon and Eric Firing provided substantial help in processing the ADCP data. The altimeter products were produced by the CLS Space Oceanography Division as part of the Environment and Climate EU ENACT project (EVK2-CT2001-00117) and with support from CNES. Tommy Dickey, Francesco Nencioli, and Will Black from

OPL-UCSB graciously provided the data for Fig. 7. Comments provided by two anonymous reviewers helped to improve the initial manuscript. Paulo H.R. Calil gratefully acknowledges support from Coordenação de Aperfeiçoamento de Pessoal de Nível Superior (CAPES), Ministry of Education of Brazil, through a Ph.D. fellowship (Process: 1526-02-2). Kelvin J. Richards and Yanli Jia were supported by NOAA Grant NA17RJ1230. This is SOEST publications number 7137 and IPRC publication number 462.

References

Beckmann, A., Haidvogel, D., 1993. Numerical simulation of flow around a tall isolated seamount, part i: problem formulation and model accuracy. Journal of Physical Oceanography 23, 1736–1753.

Benitez-Nelson, C.R., Bidigare, R.R., Dickey, T.D., Landry, M.R., Leonard, C.L., Brown, S.L., Nencioli, F., Rii, Y.M., Maiti, K., Becker, J.W., Bibby, T.S., Black, W., Cai, W.-J., Carlson, C.A., Chen, F., Kuwahara, V.S., Mahaffey, C., McAndrew, P.M., Quay, P.D., Rappe, M.S., Selph, K.E., Simmons, M.P., Yang, E.J., 2007. Mesoscale eddies drive increased silica export in the subtropical pacific ocean. Science 316 (5827), 1017–1021.

Chao, Y., Li, Z., Kindle, J.C., Paduan, J.F., Chavez, F.P., 2003. A high-resolution surface vector wind product for coastal oceans: blending satellite scatterometer measurements with regional mesoscale atmospheric model simulations. Geophysics Research Letters 30 (1).

Chavanne, C., Flament, P., Lumpkin, R., Dousset, B., Bentany, A., 2002. Scatteromete observations of wind variations induced by oceanic islands: implications for a wind-driven ocean circulation. Canadian Journal of Remote Sensing 28, 466–474.

Chen, S., Qiu, B., 2006. Trapped annual rossby waves northeast of the Hawaiian Islands. Geophysical Research Letters 33, 1–2.

Conkright, M.E., Locarnini, R.A., Garcia, H.E., O'Brien, T.D., Boyer, T.P., Stephen, C., Antonov, J.I., 2002. World ocean atlas 2001: objective analyses, data statistics, and figures. Technical Report, National Oceanographic Data Center, Silver Spring, MD, 17pp.

Dickey, T., Nencioli, F., Kuwahara, V., Leonard, C., Black, W., Bidigare, R., Rii, Y., Zhang, Q., 2007. Physical and bio-optical observations of oceanic cyclones west of the island of hawaiis. Deep-Sea Research, in press, doi:10.1016/j.dsr2.2008.01.006.

Dong, C., McWilliams, J., Shchepetkin, A., 2007. Island wakes in deep water. Journal of Physical Oceanography 37, 862–891.

Firing, E., Qiu, B., Miao, W., 1999. Time-dependent island rule and its application to the time-varying north Hawaiian ridge current. Journal of Physical Oceanography 29, 2671–2688.

Flament, P., Lumpkin, R., Tournadre, J., Armi, L., 2001. Vortex pairing in an unstable anticyclnic shear flow: discrete subharmonics of one pendulum day. Journal of Fluid Mechanics 440, 401–409.

Godfrey, J.S., 1989. A sverdrup model of the depth-integrated flow of the world ocean allowing for island circulations. Geophysical and Astrophysical Fluid Dynamics 45, 89–112.

Graves, L., McWilliams, J., Montgomery, M., 2006. Vortex evolution due to straining: a mechanism for dominance of strong, interior anticyclones. Geophysical and Astrophysical Fluid Dynamics 100 (3), 151–183.

Hafner, J., Xie, S.P., 2003. Far-field simulation of the Hawaiian wake: sea surface temperature and orographic effects. Journal of Atmospheric Sciences 60, 3021–3032.

Kobashi, F., Kawamura, H., 2002. Seasonal variation and instability nature of the north pacific subtropical countercurrent and the Hawaiian lee countercurrent. Journal of Geophysical Research 107 (C11), 3185.

Kuwahara, V., Nencioli, F., Dickey, T., Rii, Y., Bidigare, R., 2007. Physical dynamics and biological implications of cyclone Eddy/Noah/ in the lee of Hawaii during E-Flux i. Deep-Sea Research, in press, doi:10.1016/j.dsr2.2008.01.007.

Large, W.G., Pond, S., 1981. Open ocean momentum flux measurements in moderate to strong winds. Journal of Physical Oceanography 11, 324–336.

Lukas, R., Santiago-Mandujano, F., 2001. Extreme water mass anomaly observed in the Hawaii ocean time-series. Geophysical Research Letters 28 (15), 2931–2934.

Lumpkin, C.F., 1998. Eddies and currents in the Hawaiian Islands. Ph.D. Thesis, SOEST—School of Ocean and Earth Science and Technology, University of Hawaii at Manoa, 282pp.

Mahadevan, A., Tandon, A., 2006. An analysis of mechanisms for submesoscale vertical motion at ocean fronts. Ocean Modelling 14, 241–256.

Marchesiello, P., McWilliams, J.C., Shcheptekin, A.F., 2001. Open boundary conditions for long-term integration of regional ocean models. Ocean Modelling 3, 1–20.

Marchesiello, P., McWilliams, J.C., Shcheptekin, A.F., 2003. Equilibrium structure and dynamics of the california current system. Journal of Physical Oceanography 33, 753–783.

McCreary, J., Lee, H., Enfield, D., 1989. The response of the coastal ocean to strong offshore winds: with application to circulations in the Gulfs of Tehuantepec and Papagayo. Journal of Marine Research 47, 81–109.

McGillicuddy, D., Robinson, A.R., 1997. Eddy-induced nutrient supply and new production in the Sargasso sea. Deep-Sea Research 44, 1427–1450.

Mitchum, G.T., 1995. The source of the 90-day oscillations at wake island. Journal of Geophysical Research 100, 2459–2475.

Nencioli, F., Kuwahara, V., Dickey, T.D., Rii, Y., Bidigare., R., 2007. Physical dynamics and biological implications of a mesoscale eddy in the lee of Hawai'i: cyclone Opal observations during E-Flux iii. Deep-Sea Research, in press, doi:10.1016/j.dsr2.2008.02.003.

Niiler, P., 1969. On the Ekman divergence in an oceanic jet. Journal of Geophyiscal Research 74, 7048–7052.

Okubo, A., 1970. Horizontal dispersion of floatable particles in the vicinity of velocity singularities such as convergences. Deep-Sea Research 17, 445–454.

Penven, P., Echevin, V., Pasapera, J., Colas, F., Tam, J., 2005. Average circulation, seasonal cycle, and mesoscale dynamics of the peru current system: a modelling approach. Journal of Geophysical Research 110, C10021.

Penven, P., Debreu, L., Marchesiello, P., McWilliams, J., 2006. Evaluation and application of the ROMS 1-way embedding procedure to the central California upwelling system. Ocean Modelling 12, 157–187.

Qiu, B., Koh, D.A., Lumpkin, C., Flament, P., 1997. Existence and formation mechanism of the north Hawaiian ridge current. Jounal of Physical Oceanography 27, 431–444.

Seki, M., Polovina, J., Brainard, R., Bidigare, R., Leonard, C., Foley, D., 2001. Biological enhancement at cyclonic eddies tracked with goes thermal imagery in Hawaiian waters. Geophysical Research Letters 28, 1583–1586.

Shchepetkin, A., McWilliams, J., 1998. Quasi-monotone advection schemes based on explicit locally adaptive dissipation. Monthly Weather Review 126 (6), 1541–1580.

Shchepetkin, A., McWilliams, J.C., 2003. A method for computing horizontal pressure-gradient force in an oceanic model with a nonaligned vertical coordinate. Journal of Geophysical Research 108 (C3).

Shchepetkin, A., McWilliams, J.C., 2005. The regional oceanic modelling system (roms): a split-explicit, free-surface, topography-following-coordinate oceanic model. Ocean Modelling 9, 347–404.

Smith, R.B., Grubisic, V., 1993. Aerial observations of the hawaii's wake. Journal of Atmospheric Sciences 50, 3,728–3,750.

Stern, M., 1965. Interaction of a uniform wind stress with a geostrophic vortex. Deep-Sea Research 12, 355–367.

Tang, W., Liu, W.T., Stiles, B.W., 2004. Evaluation of high-resolution ocean surface vector winds measured by quikscat scatterometer in

coastal regions. IEEE Transactions of Geosciences and Remote Sensing 42, 1762–1769.

Thomas, L., Rhines, P., 2002. Nonlinear stratified spin-up. Journal of Fluid Mechanics 473, 211–244.

Weiss, J., 1991. The dynamics of enstrophy transfer in two-dimensional hydrodynamics. Physica D 48, 272–294.

Xie, S.P., Liu, W.T., Monaka, M., 2001. Far-reaching effects of the Hawaiian Islands on the pacific ocean atmosphere system. Science 292, 2057–2069.

Yang, Y., Chen, Y.-L., Fujioka, F.M., 2005. Numerical simulations of the island-induced circulations over the island of hawaii during harp. Monthly Weather Review 133, 3693–3713.